



MIT Open Access Articles

Ultra-wide bandwidth piezoelectric energy harvesting

The MIT Faculty has made this article openly available. ***Please share*** how this access benefits you. Your story matters.

Citation	Hajati, Arman, and Sang-Gook Kim. "Ultra-wide Bandwidth Piezoelectric Energy Harvesting." Applied Physics Letters 99.8 (2011): 083105. Web. © 2011 American Institute of Physics.
As Published	http://dx.doi.org/10.1063/1.3629551
Publisher	American Institute of Physics
Version	Final published version
Accessed	Sat Jan 20 15:45:37 EST 2018
Citable Link	http://hdl.handle.net/1721.1/75264
Terms of Use	Article is made available in accordance with the publisher's policy and may be subject to US copyright law. Please refer to the publisher's site for terms of use.
Detailed Terms	

Ultra-wide bandwidth piezoelectric energy harvesting

Arman Hajati^{1,a)} and Sang-Gook Kim²

¹Department of EECS, Massachusetts Institute of Technology, Cambridge, Massachusetts 02139, USA

²Department of Mechanical Engineering, Massachusetts Institute of Technology, Cambridge, Massachusetts 02139, USA

(Received 3 January 2011; accepted 4 August 2011; published online 23 August 2011)

Here, we present an ultra wide-bandwidth energy harvester by exploiting the nonlinear stiffness of a doubly clamped microelectromechanical systems (MEMSs) resonator. The stretching strain in a doubly clamped beam shows a nonlinear stiffness, which provides a passive feedback and results in amplitude-stiffened Duffing mode resonance. This design has been fabricated into a compact MEMS device, which is about the size of a US quarter coin. Based on the open circuit voltage measurement, it is expected to have more than one order of magnitude improvement in both bandwidth (more than 20% of the peak frequency) and power density (up to 2 W/cm³) in comparison to the devices previously reported. © 2011 American Institute of Physics. [doi:10.1063/1.3629551]

In order to circumvent the “Gain-Bandwidth Dilemma,” which prevents most cantilever-based energy harvesters from practical applications,^{1–5} we utilize the stretching strain in thin, doubly clamped beams instead of the bending strain in cantilever structures.^{6,7} Consider the large deflection of a doubly clamped beam as shown in Figure 1(a). Each beam is clamped between the support and the proof mass. Pure bending requires a lateral motion of the proof mass toward the support to keep the beam’s length unchanged. However, the symmetry of the doubly clamped beam prevents any lateral and rotational motion of the proof mass other than its vertical motion. Therefore, a stretching force results in a doubly clamped structure to compensate for the inevitable increase of the beam length. A large deflection of the proof mass results in two kinds of strain: bending strain, S_B , and stretching strain, S_S .

While the bending strain is not uniform and varies along the length and across the thickness of the beam in either tension or compression, the stretching strain is always tensile and almost uniform across the length and thickness for both upward and downward motion.

The load-deflection characteristic of the doubly clamped beam can be modeled as an amplitude-stiffened Duffing spring.⁸ The elastic force can be divided into two parts: a linear term which is the result of the small deflection bending and also the residual stress in the beam and a nonlinear term which results from the stretching. For very thin and long structures (e.g., diaphragms), the structure behaves like a tensional wire. Especially, in the case of microelectromechanical system (MEMS) structures, the membrane is sufficiently thin that the bending-based linear term may be neglected.

The wide bandwidth resonance of the system can be explained by the negative feedback resulting from Duffing stiffening. Stretching stiffness induces an amplitude-dependent stiffness, $k_{eq} = (k_B + k_\sigma) + \frac{3}{4}k_S Z^2$, which forces the equivalent resonance frequency to track the excitation frequency. k_{eq} , k_B , k_σ , k_S , and Z are the equivalent linear stiff-

ness, the bending-based stiffness, the stiffness due to the residual stress, the stretching-based stiffness, and the amplitude of deflection, respectively. To achieve a stronger nonlinearity for a wider resonance bandwidth, the equivalent stiffness should be mainly controlled by the nonlinear stiffness term, such that $k_B + k_\sigma \ll k_S Z^2$. For a MEMS-scale resonator, the average residual stress in the beam is substantial. Consequently, design and process efforts have been made to minimize the average residual stress along the beam with optimized beam dimensions, choice of materials, and a heavy external proof mass.

Figure 1(b) depicts the schematic structure of our ultra-wide bandwidth (UWB) energy harvester. It consists of four identical doubly clamped beams which are connected to a single external proof mass on top of each beam’s centroid. This device is micro-fabricated by a combination of surface and bulk micro-machining processes, as shown in Fig. 1(c). The beams are covered with a thin film of lead-zirconate-

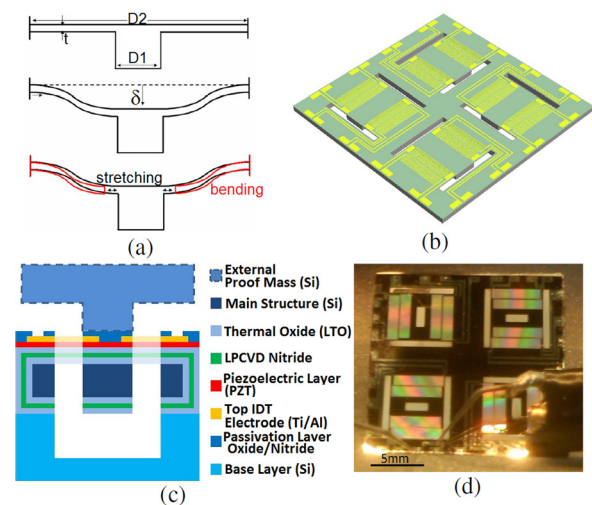


FIG. 1. (Color online) Ultra-wide bandwidth energy harvester (a) The total strain, S_T , in a doubly clamped structure is the sum of bending strain, S_B , and stretching strain, S_S , $S_T = S_B + S_S$. (b) The main harvester part consists of four doubly clamped beams before it is assembled to an external proof mass. (c) A schematic cross-section view of the harvester. (d) Optical image of the released device.

^{a)}Author to whom correspondence should be addressed. Electronic mail: hajatia@gmail.com.

titanate (PZT) (0.27 μm thick). As depicted in Fig. 1(d), 1000 pairs of interdigitated electrodes on top of the PZT layer, which are then grouped into 16 external circuits, extract the electrical charge generated in the PZT layer via d_{33} mode piezoelectric effect.⁹

The device is micro-fabricated by a combination of surface and bulk micro-machining processes; a final beam structure is shown in Figure 1(b). Layers of thermal oxide, low pressure chemical vapor deposition (LPCVD) nitride, and low temperature oxide (LTO) are deposited to form the main structure. The active layer consists of the titanium/aluminum interdigitated (IDT) electrodes (top), PZT thin-film (middle), and a layer of ZrO_2 (bottom) as a diffusion barrier layer. A plasma-enhanced chemical vapor deposited (PECVD) layer is added to protect the active layer and also to control the residual stress. A vertically symmetric stress distribution with an average stress of less than 10 MPa is achieved to enable a strong nonlinear performance. The structural layer has been patterned by reactive ion etching (RIE) from the top and deep RIE (DRIE) from the backside. To avoid excessive stress, the structure is released using a XeF_2 silicon etching step.

The packaged device is excited by an electromagnetic shaker. The motion of the proof mass and the base is measured remotely by a Doppler-effect laser vibrometer. The nonlinear harvester shows resonance in a wider range of frequencies compared to a linear resonator with a similar Q-factor. Unlike a linear resonator, the response of the nonlinear harvester depends on the trajectory of the excitation. Ramping up the frequency pushes the resonator along the high-energy stable region, like a frequency-locked loop, then jumps down from the high-energy state to the low-energy state when instability overcomes the nonlinear stiffness feedback (Figure 2).

The piezoelectric properties of the PZT were tested by x-ray diffraction crystallography (XRD) and polarization-voltage (P-V) measurement. XRD shows that the PZT is crystallized mainly in $\langle 111 \rangle$ perovskite phase. In addition, the remnant polarization, saturation polarization, and coercive field of the device are measured to be $2P_r = 36 \mu\text{C}/\text{cm}^2$, $2P_s = 102 \mu\text{C}/\text{cm}^2$, and $2E_c = 200 \text{ kV}/\text{cm}$, respectively. The device was poled at high temperature (140 $^\circ\text{C}$) and strong electric field (400 kV/cm). To avoid electric breakdown, a limiting serial resistor was employed as a negative feedback.

The electrical properties of the fabricated device with an external silicon proof mass (180 mg) were tested to measure the energy harvesting performance. The poled device is excited by a B&K electromagnetic shaker type 4809 which is controlled by Prema ARB 1000 signal generator. Motion of the central proof mass and the base is measured remotely by a Polytec PSV-300H Doppler-effect laser vibrometer. The dielectric constant, piezoelectric constant, and piezoelectric coupling factor are estimated as $\epsilon_r = 2000$, $d_{33} = 110 \text{ pm}/\text{V}$, and $k_{33} = 20\%$, respectively.

The output open-circuit voltage was fed into a FFT analyzer and two main components were identified at each excitation frequency as shown in Figure 2. The first component is a sinusoid with a frequency matching the excitation frequency (Fig. 2(b)), which corresponds to the bending strain induced in the beams. It increases slowly as the input

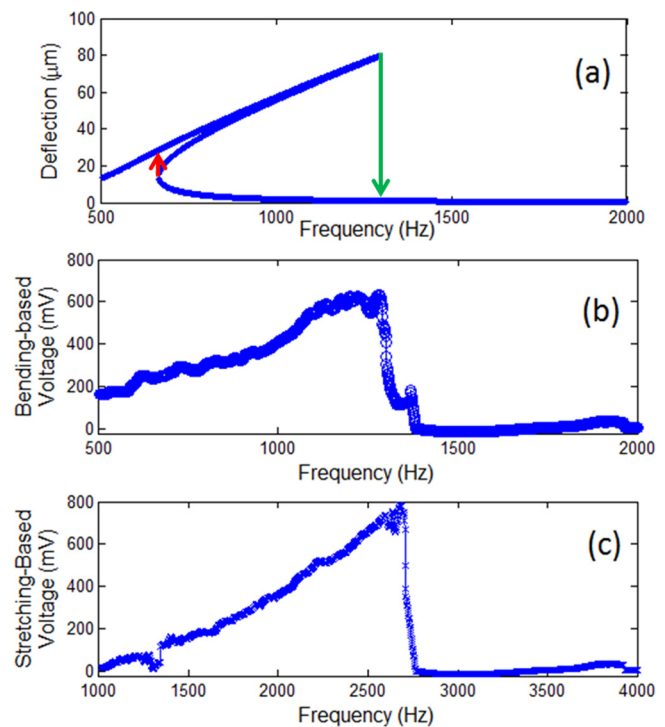


FIG. 2. (Color online) Frequency response of the UWB energy harvester. The device was mounted on the electromechanical shaker, which is driven by 1.0 V input signal. The device was excited by a sweeping sinusoid which was ramped up from 500 Hz to 2000 Hz. (a) Theoretical roots of the governing nonlinear equation of motion given by $(k_B + k_{\sigma_0})\delta + k_s\delta^3 + C(\dot{\delta}, I_{Load}) + m_{pm}\ddot{\delta} = -m_{pm}A_{ex}\sin\omega_{ext}t$, determine the deflections of the system. The jump-down and jump-up frequencies are marked by green and red arrows, respectively. (b) The output voltage generated by the energy harvester is monitored by a fast fourier transform (FFT) analyzer. For each excitation frequency, two components can be seen in the frequency domain. The first harmonic at the excitation frequency corresponds to the bending strain. (c) Another harmonic at twice the frequency of excitation is also generated due to the always-tensile stretching strain.

frequency goes up until the harvester jumps down at ~ 1350 Hz. Fig. 2(c) shows the amplitude of a second harmonic which corresponds to the charge generated due to the nonlinear mode stretching strain in the structure. Since the always-tensile strain reaches its maximum two times per input vibration cycle, this component has twice the excitation frequency. This component scales up quadratically as a function of frequency and can be regarded as the main source of power generation. This component is the key to the high-density UWB energy harvesting and cannot be seen in linear harvesters.

The electrical damping can be increased as long as the total electro-mechanical damping does not push the resonator into instability, resulting in jump-down to low energy state. At the jump-down frequency, the nonlinear feedback from the stretching stiffness is not large enough to keep the frequency-locked loop within the threshold of instability where the resonator jumps down to the low-energy stable region. Unlike a linear resonating device,¹⁰ the electrical damping (extracted electrical power) in the nonlinear energy harvester may not be bounded by the mechanical damping, which will be further investigated in the future study. More electric power can be extracted when the operational frequency is much lower than the jump-down frequency, since it can tolerate more electrical damping. Exploiting this

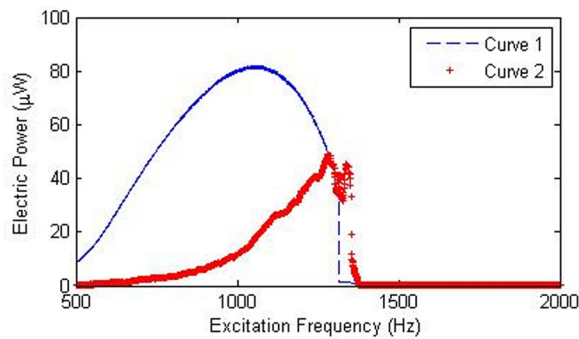


FIG. 3. (Color online) Mechanical response of the system as a function of excitation frequency. Curve 1 shows the theoretically extractable power of the nonlinear Duffing resonator based on the mechanical analysis, assuming ideal electric loading. Curve 2 depicts the generated power based on the measured open-circuit voltage.

property, theoretically extractable power is calculated as shown in curve 1 of Figure 3.

This curve shows the maximum extractable power based on adjusting the electrical load as a function of frequency. Assuming an ideal electric load, the extractable power is estimated based on the open-circuit voltage generated. Compared to the fixed load condition, the extractable power can be boosted at lower frequencies by increasing the electrical load using a synchronized switching harvesting interface (SSHI) circuit.¹¹ The nonlinear resonator shows a power (extractable) bandwidth exceeding 50% of the arithmetic center frequency while a typical linear resonator has a power bandwidth less than 1% which shows 2 orders of magnitude improvement.

A piezoelectric power source can be fully characterized as an ideal voltage source (or current source) and its internal capacitance. Accordingly, the actual generated power based on the measured open-circuit voltage (shown in Figure 2) and the internal capacitance (8.5 nF) and resistance (3.5 M Ω) is shown as curve 2 in comparison to the maximum theoretically extractable power (curve 1). The generated power is based on only one layer of PZT (265 nm) and a SSHI,¹¹ with effective Q_I of 20 and shows a bandwidth exceeding 20% of the arithmetic center frequency. Unlike a pure resistive loading, a switching inductor is employed to improve the efficiency of electric power extraction up to $P_{\max} = \frac{Q_I^2 I_p^2}{4\pi^2 C_0 \omega_{ex}}$ in which I_p , C_0 , and ω_{ex} are the piezoelectric current source, the internal capacitance, and the excitation frequency, respectively. The generated power is scaled by the mechanical-to-electrical coupling property and the thickness of the PZT layer and also the efficiency of the electrical interface. The actual generated power in this case is smaller than the maximum extractable power, which can be easily scaled up by placing more (or thicker) layers of PZT and adjusting the electric load to exploit the high electrical damping capacity of the non-linear beam. Considering the

volume of PZT ($4 \times 5 \text{ mm} \times 4 \text{ mm} \times 265 \text{ nm} \approx 0.021 \text{ mm}^3$), the generated power density is 2 W/cm^3 . This level of power density is at least two orders higher than the previously reported piezoelectric energy harvesters.¹

The power generation capability of a similar device but with a misaligned electrode is tested with direct resistive loads. Stretching strain in the beam between the electrodes would result in 5 times smaller strain (the effective Poisson's ratio) and gives 5 times smaller voltage (and 25 times smaller power) output than those of the correct device. At 450 Hz, the tested device generates 140 nW of power measured across the optimal resistive load of 290 k Ω . By correcting the electrode orientation and improving the device quality, we improved the open circuit voltage by more than 7 times (up to 0.8 V) at 1.3 kHz as reported in Figure 2. Considering a similar capacitance and impedance for both devices, the extractable electric power by an optimal direct resistive load would be 22 μW which compares well with the expected power of 45 μW shown in Figure 3.

Harvesting power from environmentally available vibration will be useful for applications where no power sources other than chemical battery are available. Toward this end, energy harvesting from vibrations should overcome the two biggest challenges: maintaining resonance over an uncertain spectrum of environmental vibration (wide bandwidth) and high power density to ensure compact and low-cost device manufacturing. The piezoelectric energy harvester with doubly clamped beam structures has demonstrated both wide enough bandwidth resonance and high enough power density. The wireless sensor community has long sought to achieve a sustainable power source of more than 100 μW continuous at the size of a small coin. The power estimated from the measured open circuit voltage of our device is 45 μW , which would be increased to 85 μW with a smart adaptive interface, and more than 100 μW by doubling the piezoelectric layers to draw more electrical energy already available in the nonlinear beam. 1000 μW directly measured power at the same size of the device is our near-term goal in making practically deployable energy harvesters.

¹S. P. Beeby, M. J. Tudor, and N. M. White, *Meas. Sci. Technol.* **17**, 175 (2006).

²S. Roundy, P. Wright, and J. Rabaey, *Comput. Commun.* **26**, 1131 (2003).

³P. Muralt, M. Marzencki, B. Belgacem, F. Calame, and S. Basrour, *Procedia Chemistry*, **1**, 1191 (2009).

⁴A. Erturk and D. Inman, *J. Intell. Mater. Syst. Struct.* **19**, 1311 (2008).

⁵Y. Jeon, R. Sood, J. Jeong, and S. G. Kim, *Sens. Actuators, A* **122**, 16 (2005).

⁶A. Hajati and S. G. Kim, *Proc. SPIE* **6928**, 69281T (2008).

⁷B. Marinkovic and H. Koser, *Appl. Phys. Lett.* **94**, 103505 (2009).

⁸S. D. Senturia, *Microsystem Design* (Springer, New York, 2004), pp. 249–252.

⁹S. Trolier-McKinstry and P. Muralt, *J. Electroceram.* **12**, 7 (2004).

¹⁰N. duToit, B. Wardle, and S. G. Kim, *Integr. Ferroelectr.* **71**, 121 (2005).

¹¹D. Guyomar, A. Badel, E. Lefeuvre, and C. Richard, *IEEE Trans. Ultrason. Ferroelectr. Freq. Control* **52**, 584 (2005).